A Learning-Based Hierarchical Control Scheme for an Exoskeleton Robot in Human–Robot Cooperative Manipulation

Mingdi Deng, Zhijun Li, *Senior Member, IEEE*, Yu Kang, *Senior Member, IEEE*, C. L. Philip Chen, *Fellow, IEEE*, and Xiaoli Chu

***Abstract*—Exoskeleton robots can assist humans to perform activities of daily living with little effort. In this paper, a hierarchical control scheme is presented which enables an exoskeleton robot to achieve cooperative manipulation with humans. The control scheme consists of two layers. In low-level control of the upper limb exoskeleton robot, an admittance control scheme with an asymmetric barrier Lyapunov function-based adaptive neural network controller is proposed to enable the robot to be back drivable. In order to achieve high-level interaction, a strategy for learning human skills from demonstration is proposed by utilizing Gaussian mixture models, which consists of the learning and reproduction phase. During the learning phase, the robot observes and learns how a demonstrator performs a specific impedance-based task successfully, and in the reproduction phase, the robot can provide the subjects with just enough assistance by extracting human skills from demonstrations to prevent the motion of the robot end-effector deviating far from desired ones, due to variation in the interaction force caused by environmental disturbances. Experimental results of two different tasks show that the proposed control scheme can provide human subjects with assistance as needed during cooperative manipulation.**

***Index Terms*—Asymmetric barrier Lyapunov function (ABLF), exoskeleton robot, Gaussian mixture, human–robot cooperative manipulation, impedance-based task, learning human skills from demonstration.**

I. Introduction

OVER THE past decades, exoskeleton robots have been developed for human power augmentation and rehabilitation training [1]. One of the most critical issues in controlling a robotic exoskeleton is to enable the robots to learn the human's experiences and skills so that the robots could actively cooperate with the human subject. In this paper, a hierarchical control scheme is proposed, which includes a high-level learning model for interaction that can learn human experience and skills from demonstration, and low-level robot motion control that enables the robot to be back drivable. One way to achieve successful and safe human–robot cooperative manipulation is to make the robot possess the ability of estimating human intention. There are multiple types of information that a robot could use to predict human intention, including motion, partner posture, and interaction force between the human and environment among others [4]. For example, electromyography (EMG) signals, generated by motor neuron impulses that activate the muscle fibers, can be correlated with the torque at the joint level produced by muscles [2], which contains the human intention information.

The EMG-based intention estimation methods are related to complex calibrations that are necessary for accurate and reliable modeling. The relation between EMG signals and torques involves several nonlinearities and strongly depends on the placement of electrodes [3]. Compared to model-based methods, EMG-based techniques do not require a dynamic model of the limb interaction with the environment. An alternative to estimating human intention is to enable the robot to learn from demonstrations and transfer the human experience and skills from demonstrations to the robot.

Until now, there are many different approaches investigated for learning from demonstration (LfD). For example, learning algorithms such as hidden Markov models (HMMs) and GMM have been used in [5]–[8]. In [5], a prediction framework based on HMMs was proposed to estimate the human's intended trajectory, which employs a position-based impedance controller to map the haptic observations to the estimated trajectory. In [6], online incremental learning of

Manuscript received January 2, 2018; revised April 10, 2018, June 10, 2018, and July 13, 2018; accepted August 4, 2018. This work was supported in part by the National Natural Science Foundation of China under Grant 61573147, Grant 61625303, and Grant 61751310, in part by the Guangdong Science and Technology Research Collaborative Innovation Projects under Grant 2014B090901056, Grant 2015B020214003, and Grant 2016A020220003, in part by the Guangdong Science and Technology Plan Project (Application Technology Research Foundation) under Grant 2015B020233006, and in part by the Anhui Science and Technology Major Program under Grant 17030901029. This paper was recommended by Associate Editor Z. Ju. *(Corresponding author: Zhijun Li.)*

M. Deng is with the College of Automation Science and Engineering, South China University of Technology, Guangzhou 510640, China (e-mail: deng890614@126.com).

Z. Li was with the College of Automation Science and Engineering, South China University of Technology, Guangzhou 510640, China. He is now with the Department of Automation, University of Science and Technology of China, Hefei 230027, China (e-mail: zjli@ieee.org).

Y. Kang and X. Chu are with the Department of Automation, University of Science and Technology of China, Hefei 230027, China (e-mail: kangduyu@ustc.edu.cn).

C. L. P. Chen is with the Faculty of Science and Technology, University of Macau, Macau 999078, China (e-mail: philip.chen@ieee.org).

Color versions of one or more of the figures in this paper are available online at http://ieeexplore.ieee.org.

Digital Object Identifier 10.1109/TCYB.2018.2864784

full body motion primitives was proposed, which partitioned human motion trajectory into motion primitives and then used an HMM to encode each motion primitive. In [7], several sets of trajectories were modeled by a library of GMMs, and the human intention inference algorithm was developed using unsupervised GMMs. In [8], the application of a statistical framework was presented, which endows a robot with the ability to perform a cooperative manipulation task with a human subject. In [9], a comprehensive survey of robot LfD, a technique that develops policies from example state to action mappings, has been presented. In [10], dynamical movement primitives (DMPs) for modeling attractor behaviors of autonomous nonlinear dynamical systems have been presented. However, the above works seldom consider the variability of human–robot cooperative manipulation among multiple demonstrations or exploit it in the reproduction phase.

When a human subject interacts with a robot, one goal is to model the human behavior which is recorded during demonstration, and to determine the underlying features and constraints of the interaction. During demonstration, a demonstrator teaches a robot how to execute the task successfully and allows it to analyze the behavior recorded by using statistical approaches such as what follows.

In this paper, a strategy for learning human skills from demonstration that utilizes GMM for high-level interaction is presented. In human–robot cooperative manipulation, the human subject should offer a minimum impedance required to complete a cooperative task. But due to variation in the interaction force caused by environmental disturbances, the motion of the robot end-effector would deviate far from the desired, which may lead to the failure of the task. The proposed strategy for learning human skills from demonstration compares the impedance behavior of a demonstrator in those successful trials with that of the subjects who want to perform the same task. First during demonstration, the demonstrator performs the tasks individually and successfully. The underlying features and constraints of the interaction are statistically analyzed and learned using GMM based on logged human–robot interaction data. Then, during reproduction, the robot predicts the interaction force similar to those in demonstrations by using Gaussian mixture regression (GMR), to assist the subjects with external assistance to be sure that the task can be completed successfully. To encourage the subjects to actively participate into the cooperative task, provision of assistance to the subject is adjusted according to the variability of the demonstrator's behavior observed in the demonstration phase. Therefore, the presented learning-based strategy transfers the underlying characteristics and constraints of the given impedance-based task to the exoskeleton robot, which leads to cooperative interaction between the human subject and the robot, where the robot provides assistance only when needed. Furthermore, we extended the learning model to task-parameterized GMM [29] in order to reproduce motions with different targets.

On the other hand, low-level motion control of the robot needs to be designed to achieve comfortable and safe interaction with the robot. In [12], in order to design an admittance control when the model of the exoskeleton robot is unavailable, a model-free PID-type admittance control has been proposed. In [13], in order to achieve the goal of the operator feeling as if a wearable robot is a natural extension of the body, a novel admittance control for a wearable robot has been developed. However, these works do not consider the physical constraints of an upper limb exoskeleton. Various physical constraints such as safety specifications and physical limits normally exist in many robotic systems [14]–[16]. Violation of constraints may degrade the performance of the system. For example, the maximum value of a robotic manipulator's joint position is constrained by its physical configuration and it needs to avoid violating this physical limits when it operates. Without taking constraints into account, the control design would lead to the failure of control. Therefore, it is a challenge to deal with the constraint as one of the control objectives. Many methods have been proposed to handle the constraints problem for various mechanical systems. In [17], contractive model predictive control was proposed for constrained nonlinear systems. In [18], to handle the constraints in robotic systems, a barrier Lyapunov function (BLF) was developed. In [19], a systematic control design for single-input–single-output (SISO) nonlinear systems with output constraints was presented. BLF is used for the SISO output-constrained nonlinear system in [20], and in [21], it is used for the nonlinear system with time-varying constraints. In [22], a novel integral BLF is designed for the control of an SISO nonlinear system with state constraints. As we can see from the above works, the BLF method has been proven to be an effective method in the control of robotic system with constraints. However, none of these works considers human–robot interaction for a robotic exoskeleton, nor the use of asymmetric BLF (ABLF).

For low-level robot motion control, this paper proposed an admittance control scheme with an inner position controller. Admittance control provides an established mechanism to specify a dynamic relationship between position and force in a system, and provides definable degrees of compliance. The admittance control uses the interaction force as input and outputs the position of the robot end-effector in task space, and it requires an inner position controller to track this position. In order to avoid singularities in task space so that the robot can operate without violating asymmetric physical constraints, and to improve the tracking performance, we designed an ABLF-based adaptive neural network (NN) controller, which allows the tracking errors to remain within the constraints. ABLF is used to cope with asymmetric physical constraints while adaptive NN is used to approximate the unknown model parameters of the robotic system.

In this paper, we present a learning-based hierarchical control scheme which consists of a high-level learning model that is capable of characterizing cooperative impedance-based manipulation tasks, and a low-level admittance controller with an inner position controller that is able to deal with asymmetric constraints. The robot first observes and learns the impedance-based behavior of the demonstrator in the demonstration phase, and then predicts the movements the subject should have based on recorded demonstrated motion data so that it can assist the subject by compensating for the

differences between predicted movements and the subject's actual movements during reproduction.

The contributions of this paper are threefold:

1) a newly designed ABLF-based adaptive NN controller that achieves asymptotic tracking without violating asymmetric output constraints and its application in an exoskeleton robot;
2) a learning-based control scheme which guides exoskeleton robot to aid human with assistance only when needed;
3) extension of task-parameterized GMM into human–robot cooperative manipulation for exoskeleton robot.

II. Proposed Approach for Human–Robot Interaction

In human–robot cooperative manipulation settings, a robot physically interacts with humans through its end-effector. For such cooperative tasks, it would not be safe to use traditional position control without considering the environment with which the robot interacts, especially with a human, which is very hard to model. Thus, various dynamic models of physical interaction between the end-effector and the environment, such as impedance control techniques, have been proposed in [24]–[26]. In order to describe the robot's desired motion during interaction with the environment, the end-effector is treated equivalently as a single unit mass which is driven by a virtual spring–damper system and moving in task space. The models ensure that the dynamics of the robot interacts with its environment through this virtual mass–spring–damper system such that

$$f_{\text{int}} = \lambda(\ddot{\mathbf{x}}_r - \ddot{\mathbf{x}}_h) + \Psi(\dot{\mathbf{x}}_r - \dot{\mathbf{x}}_h) + \Gamma(\mathbf{x}_r - \mathbf{x}_h) \tag{1}$$

where $\mathbf{x}_h$ is the position of the virtual attractor, $\mathbf{x}_r$ is the position of the end-effector, and f_{int} is the interaction force exerted on the end-effector. Λ, Ψ, and Γ that can be preselected are, respectively, the desired inertia, damping, and stiffness matrices of the mass–spring–damper system.

In [8] and [26], the control law expressed in (1) is simplified as follows:

$$\ddot{\mathbf{x}}_r = \Gamma(\mathbf{x}_h - \mathbf{x}_r) - \Psi\dot{\mathbf{x}}_r + f_{\text{int}} \tag{2}$$

where f_{int} can be measured by the force sensor and $\mathbf{x}_r$, $\dot{\mathbf{x}}_r$, and $\ddot{\mathbf{x}}_r$ are measured by robot encoders.

The proposed approach is illustrated in Fig. 1. During the learning phase, the demonstrator first performs multiple successful trials of the desired task, and the dataset of each trial measured by the force sensor and robot encoders is stored. Then the stored dataset is preprocessed by (2) to obtain dataset $\mathcal{Y}$, and it is then used to train GMM parameters by using the expectation-maximization (EM) algorithm offline, as shown in the dashed block of the learning phase. Once GMM is trained, the robot can use it to predict cooperation movements, as shown in the dashed block of the reproduction phase. Equation (2) is also used to calculate $\mathbf{x}_h$, and GMR based on the trained GMM is applied to predict the expected interaction force between robot and human, given the current time t and $\mathbf{x}_h$. The assistance is then calculated by a PID force controller,

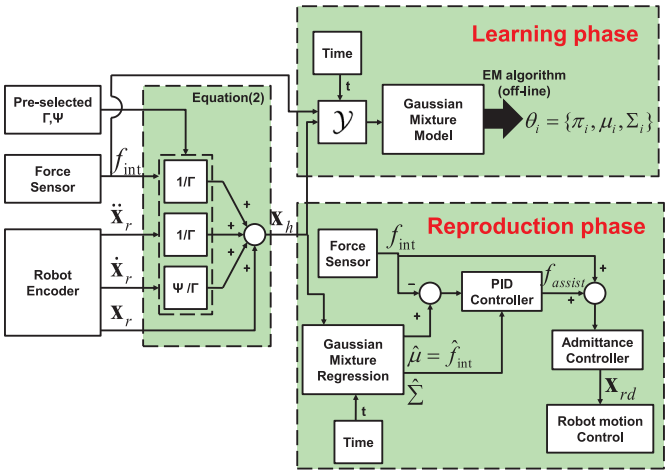

Fig. 1. Block diagram of the scheme for learning human skills from demonstration. Top: Learning phase of the hierarchical control scheme. Bottom: Reproduction phase of the hierarchical control scheme.

and it is compared to the actual force to obtain the input of an admittance controller, by which we can obtain the desired position $\mathbf{x}_{rd}$ of the end-effector which is the input of a controller to be designed.

Table I is used as a reference to the notation and names of variables used in this paper, and vectors or matrices related to the interaction force, position of the virtual attractor, and time will be added to the superscript of r, h, and t, respectively, in the following sections.

A. Learning Model

GMM is a mixture model of K Gaussian distributions and is used to approximate the joint distribution of the cooperative task

$$f_{R,H,T}(r,h,t) = \sum_{i=1}^{K} \pi_i \phi(y|\mu_i, \Sigma_i) \tag{3}$$

with

$$\mu_i = \begin{bmatrix} \mu_i^r \\ \mu_i^h \\ \mu_i^t \end{bmatrix}, \begin{matrix} \mu_i^r \in \mathbf{R}^m \\ \mu_i^h \in \mathbf{R}^m \\ \mu_i^t \in \mathbf{R}^1 \end{matrix}, \Sigma_i = \begin{bmatrix} \Sigma_i^{rr} & \Sigma_i^{rh} & \Sigma_i^{rt} \\ \Sigma_i^{hr} & \Sigma_i^{hh} & \Sigma_i^{ht} \\ \Sigma_i^{tr} & \Sigma_i^{th} & \Sigma_i^{tt} \end{bmatrix}. \tag{4}$$

The parameters of GMM can be denoted by $\boldsymbol{\theta} = (\theta_1, \theta_2, \ldots, \theta_K)$, where $\theta_i = \{\pi_i, \mu_i, \Sigma_i\}$ with constraint $\sum_{i=1}^{K} \pi_i = 1 \quad , \forall i : \pi_i \geq 0$. These parameters are estimated using $\mathcal{Y}$ by the standard EM algorithm [28].

GMR is then used to calculate the conditional probability $f_{R|H,T}(r|h,t)$ at each time step during reproduction, in other words, to predict the expected interaction force given new position and time data. To derive this probability, we first consider one component of the mixture model $\phi(y|\mu_i, \Sigma_i)$, and derive the parameters of its corresponding conditional density $\phi(r|h,t,\hat{\mu}_i, \hat{\Sigma}_i)$. Define $Z = R + \mathcal{A}H + \mathcal{B}T$ and we have

$$\begin{aligned} \hat{\mu}_i &= E(Z - \mathcal{A}H - \mathcal{B}T | H = h, T = t) \\ &= E(Z|H = h, T = t) - \mathcal{A}h - \mathcal{B}t \\ &= E(Z) - \mathcal{A}h - \mathcal{B}t \\ &= \mu_i^r + \mathcal{A}\mu_i^h + \mathcal{B}\mu_i^t - \mathcal{A}h - \mathcal{B}t. \end{aligned}$$

TABLE I
NOTATION AND NAMES OF VARIABLES

$f_{int}, \hat{f}_{int}$	Measured and predicted interaction force exerted on the robot end-effector
$\mathbf{x}_h$	Position of the virtual attractor in task space
$\mathbf{x}_r, \mathbf{x}_{rd}$	Measured and desired position of the robot end-effector in task space
Λ, Ψ, Γ	Desired inertia, damping and stiffness matrices of the mass-spring-damper system
π_i, μ_i, Σ_i	Prior probability, mean and covariance matrix of the ith component of GMM
R, H, T	Random variables of the interaction force f_{int}, position of the virtual attractor $\mathbf{x}_h$ and time t
r, h, t	Sample of R, H, T with $r, h \in \mathbf{R}^m$, and $t \in \mathbf{R}^1$
y	Sample of one data point and $y = [r^T, h^T, t]^T$
$\mathbf{y}$	Dataset of one trajectory with N data points and $\mathbf{y} = \{y_n\}_{n=1}^N$
$\mathcal{Y}$	Dataset of M trajectories and $\mathcal{Y} = \{\mathbf{y}_i\}_{i=1}^M$
$\phi(y\|\mu_i, \Sigma_i)$	Gaussian distribution with mean μ_i and covariance matrix Σ_i
$\varpi_i, \hat{\mu}, \hat{\Sigma}$	Prior probability, mean and covariance matrix of the GMR
$\mathcal{R}_j, b_j$	Orientation matrix and position vector of the initial/target point
$\pi_i, \mathbf{Z}_{i,j}^{\mu}, \mathbf{Z}_{i,j}^{\Sigma}$	Prior probability, mean and covariance matrices of ith component and jth task parameters
$\mathbf{M}_d, \mathbf{C}_d$	Desired virtual inertia and virtual damping diagonal matrices of admittance controller
f_{assist}	Assistive force by PID force controller
K, I, D	Gains of the proportional, integral and derivative term of PID force controller
q	Position in joint space with $q = [q_1, q_2, \cdots, q_n]^T \in \mathbf{R}^n$
$f(q), f^{-1}(\mathbf{x}_r)$	Forward kinematics function with $\mathbf{x}_r = f(q)$ and inverse kinematics function with $q = f^{-1}(\mathbf{x}_r)$
$M(q)$	Inertia matrix of the robot dynamics and $M(q) \in \mathbf{R}^{m\times n}$
$C(q, \dot{q})$	Coriolis and centripetal coupling matrix of the robot dynamics and $C(q, \dot{q}) \in \mathbf{R}^{m\times n}$
$F(\dot{q})$	Friction force in robot dynamics and $F(\dot{q}) \in \mathbf{R}^m$
$G(q)$	Gravity loading in robot dynamics and $G(q) \in \mathbf{R}^m$
$J(q)$	Jacobian matrix of the robot and $J(q) \in \mathbf{R}^{m\times n}$
τ, τ_{int}	Torques of the joints applied by the robot and the human, and $\tau_{int} = J(q)^T f_{int}$
$\mathbf{0}, I$	Zero vector and Identity matrix

This holds only when Z is independent of both H and T. This can be achieved by finding $\mathcal{A}$ and $\mathcal{B}$ such that

$$\begin{cases} \text{cov}(Z, H) = 0 \\ \text{cov}(Z, T) = 0 \end{cases}$$

and the solution is

$$\begin{cases} \mathcal{A} = \left(\Sigma_i^{rh} - \Sigma_i^{rt}\Sigma_i^{tt^{-1}}\Sigma_i^{th}\right)\left(\Sigma_i^{ht}\Sigma_i^{tt^{-1}}\Sigma_i^{th} - \Sigma_i^{hh}\right)^{-1} \\ \mathcal{B} = \left(\Sigma_i^{rt} - \Sigma_i^{rh}\Sigma_i^{hh^{-1}}\Sigma_i^{ht}\right)\left(\Sigma_i^{th}\Sigma_i^{hh^{-1}}\Sigma_i^{ht} - \Sigma_i^{tt}\right)^{-1}. \end{cases} \tag{5}$$

Therefore, we have

$$\hat{\mu}_i = \mu_i^r + \mathcal{A}\mu_i^h + \mathcal{B}\mu_i^t - \mathcal{A}h - \mathcal{B}t. \tag{6}$$

The variance $\hat{\Sigma}_i = \text{var}(R|H = h, T = t)$ can also be calculated by using independence between Z and R/T, and the result is

$$\hat{\Sigma}_i = \Sigma_i^{rr} + \mathcal{A}\Sigma_i^{ht}\mathcal{A}^T + \mathcal{B}\Sigma_i^{tt}\mathcal{B}^T + \mathcal{A}\Sigma_i^{ht}\mathcal{B}^T + \mathcal{B}\Sigma_i^{th}\mathcal{A}^T. \tag{7}$$

Then, we extend one joint Gaussian density to mixture of multiple Gaussian distributions. Integrating (3) with respect to R we obtain the marginal density

$$f_{H,T}(h, t) = \sum_{i=1}^K \pi_i \phi\left(h, t|\mu_i^{h,t}, \Sigma_i^{h,t}\right) \tag{8}$$

where $\mu_i^{h,t}$ and $\Sigma_i^{h,t}$ are actually corresponding blocks of the matrices in (4). Considering (6) and (7), we rewrite (3) as

$$f_{R,H,T}(r, h, t) = \sum_{i=1}^K \pi_i \phi\left(r|h, t, \hat{\mu}_i, \hat{\Sigma}_i\right)\phi\left(h, t|\mu_i^{h,t}, \Sigma_i^{h,t}\right). \tag{9}$$

The conditional density of the GMM can be formulated by dividing (9) by (8)

$$\begin{aligned} f_{R|H,T}(r|h, t) &= \frac{f_{R,H,T}(r, h, t)}{f_{H,T}(h, t)} \\ &= \sum_{i=1}^K \varpi_i \phi\left(r|h, t, \hat{\mu}_i, \hat{\Sigma}_i\right) \end{aligned} \tag{10}$$

where

$$\varpi_i = \frac{\pi_i \phi\left(h, t|\mu_i^{h,t}, \Sigma_i^{h,t}\right)}{\sum_{j=1}^K \pi_j \phi\left(h, t|\mu_j^{h,t}, \Sigma_j^{h,t}\right)}. \tag{11}$$

The conditional expectation and covariance of the mixture model can be derived by definition according to (10) and we have

$$\hat{\mu} = \sum_{i=1}^K \varpi_i \hat{\mu}_i \tag{12}$$

$$\hat{\Sigma} = \sum_{i=1}^K \varpi_i \left(\hat{\mu}_i \hat{\mu}_i^T + \hat{\Sigma}_i\right) - \hat{\mu}\hat{\mu}^T \tag{13}$$

and we have the expected interaction force $\hat{f}_{\text{int}} = \hat{\mu}$.

B. Extension to Task-Parameterized GMM

To enable the control scheme to reproduce cooperative motion with different targets, we extend the task-parameterized movement models proposed in [29] to the case of human–robot interaction. The task parameters in this case would be $\{\mathbf{A}_j, \mathbf{b}_j\}_{j=1}^P$, where $\mathbf{A}_j = \text{diag}[1, \mathcal{R}_j, \mathcal{R}_j]$ and $\mathbf{b}_j = [0, b_j^T, \mathbf{0}]^T$, with $P = 2$.

The parameters of the task-parameterized GMM $\{\pi_i, \mathbf{Z}_{i,j}^{\mu}, \mathbf{Z}_{i,j}^{\Sigma}\}$ are estimated with a variant EM algorithm as follows. First, the probability of sample y_n is computed as

$$\sum_{i=1}^K \pi_i \phi(y_n|\mu_i, \Sigma_i) = \sum_{i=1}^K \pi_i \prod_{j=1}^P \phi\left(y_n|\mathbf{A}_j\mathbf{Z}_{i,j}^{\mu} + \mathbf{b}_j, \mathbf{A}_j\mathbf{Z}_{i,j}^{\Sigma}\mathbf{A}_j^T\right)$$

where

$$\Sigma_i = \left(\sum_{j=1}^{P}\left(\mathbf{A}_j\mathbf{Z}_{i,j}^{\Sigma}\mathbf{A}_j^T\right)^{-1}\right)^{-1}$$
$$\mu_i = \Sigma_i\sum_{j=1}^{P}\left(\mathbf{A}_j\mathbf{Z}_{i,j}^{\Sigma}\mathbf{A}_j^T\right)^{-1}\left(\mathbf{A}_j\mathbf{Z}_{i,j}^{\mu}+\mathbf{b}_j\right). \quad (14)$$

Then, the indicator variable which is one or zero according to whether y_n arose or did not arise from the ith component of the mixture in E-step is calculated as

$$\chi_{i,n} = \frac{\pi_i\phi(y_n|\mu_i,\Sigma_i)}{\sum_{k=1}^{K}\pi_k\phi(y_n|\mu_k,\Sigma_k)}$$

and the updating laws for the parameters $\{\pi_i, \mathbf{Z}_{i,j}^{\mu}, \mathbf{Z}_{i,j}^{\Sigma}\}$ in M-step are

$$\dot{\pi}_i = \frac{\sum_{n=1}^{NM}\chi_{i,n}}{NM} - \pi_i, \quad \dot{\mathbf{Z}}_{i,j}^{\mu} = \frac{\sum_{n=1}^{NM}\chi_{i,n}\mathbf{A}_j^{-1}\left(y_n-\mathbf{b}_j\right)}{\sum_{n=1}^{NM}\chi_{i,n}} - \mathbf{Z}_{i,j}^{\mu}$$
$$\dot{\mathbf{Z}}_{i,j}^{\Sigma} = \frac{\sum_{n=1}^{NM}\chi_{i,n}\mathbf{A}_j^{-1}\left(y_n-\tilde{\mu}_{i,j}\right)\left(y_n-\tilde{\mu}_{i,j}\right)^T\left(\mathbf{A}_j^{-1}\right)^T}{\sum_{n=1}^{NM}\chi_{i,n}} - \mathbf{Z}_{i,j}^{\Sigma} \quad (15)$$

with $\tilde{\mu}_{i,j} = \mathbf{A}_j\mathbf{Z}_{i,j}^{\mu} + \mathbf{b}_j$.

The EM algorithm is executed in the learning phase. During reproduction, the expected interaction force $\hat{\mu}$ and its corresponding covariance $\hat{\Sigma}$ are retrieved using GMR, and calculated by (12) and (13), but with GMM parameters $\theta_i = \{\pi_i, \mu_i, \Sigma_i\}$ calculated by (14) and (15), instead of standard EM algorithm, and the desired task parameters in reproduction can be different from those in the learning phase (see [29] for more details).

C. Admittance Control Scheme

Admittance control scheme is proposed to enable compliant motion of the exoskeleton robot. The controller establishes a second-order system relationship between the interaction force and the position of the end-effector, and uses the interaction force as input and outputs the position of the end-effector. Admittance controller can be formulated as

$$\mathbf{M}_d\ddot{\mathbf{x}}_{rd} + \mathbf{C}_d\dot{\mathbf{x}}_{rd} = f_{\text{int}} \quad (16)$$

which defines the desired behavior of the end-effector and it is adjustable. For example, if we expect the end-effector to react with a heavy damping, $\mathbf{C}_d$ is chosen to be higher value.

Note that the admittance control scheme is applied both in the phase of demonstration and reproduction, to make the robot back drivable.

D. Force Control Scheme

To determine the forces that the robot needs to provide to subjects, a PID control law can be applied as

$$f_{\text{assist}} = KE(t) + I\int_0^t E(t)dt + D\frac{dE(t)}{dt} \quad (17)$$

where $E(t) = \hat{f}_{\text{int}} - f_{\text{int}}$, and K, I, and D can be adaptively regulated according to the variability of the demonstrations such that assistance is provided only when needed

$$K(t) = K_0 - \kappa_1\left(\hat{\Sigma}^2(t) - |E(t)|\right) \quad (18)$$
$$I(t) = I_0 - \kappa_2\left(\hat{\Sigma}^2(t) - |E(t)|\right) \quad (19)$$
$$D(t) = D_0 - \kappa_3\left(\hat{\Sigma}^2(t) - |E(t)|\right) \quad (20)$$

where $\hat{\Sigma}(t)$ represents the variability of the demonstrations, which is calculated via GMR by (13); K_0, I_0, and D_0 are initial value of the controller gains; and κ_1, κ_2, and κ_3 are tunable positive constants. If the subject acts similar to the demonstrator's performance, then $|E(t)|$ is close to zero and the controller gains decrease to minimum. Otherwise, $|E(t)|$ will increase as the controller gains, which results in more assistance to the subject by the robot to bring cooperative motion back into the expected one.

E. Control Design

Lemma 1 [19]: Let $\mathcal{Z} := \{z_1 \in \mathbf{R} : -k_a < z_1 < k_b\} \subset \mathbf{R}$ and $\mathcal{N} := \mathbf{R}^l \times \mathcal{Z} \subset R^{l+1}$ be open sets, where k_a and k_b are any positive constants and l is a positive integer. Consider the system

$$\dot{z} = h(t, z)$$

where $z := [z_2, z_1]^T \subset \mathcal{N}(z_2 \in \mathbf{R}^l)$ and $h : \mathbf{R}^+ \times \mathcal{N} \to \mathbf{R}^{l+1}$ is uniformly in t, locally Lipschitz in z, and piecewise continuous on $\mathbf{R}^+ \times \mathcal{N}$. Define two functions $U : \mathbf{R}^l \times \mathbf{R}^+ \to \mathbf{R}^+$ and $V_1 : \mathcal{Z} \to \mathbf{R}^+$ that are positive definite and continuously differentiable in their respective domains such that

$$V_1(z_1) \to \infty \text{ as } z_1 \to -k_a \text{ or } z_1 \to k_b$$
$$\eta_1(\|z_2\|) \le U(z_2, t) \le \eta_2(\|z_2\|)$$

where η_1 and η_1 are class K_∞ functions. Define $V(z) := V_1(z_1, t) + U(z_2)$, and $z_1(0) \in \mathcal{Z} \in (-k_a, k_b)$. $z_1(t)$ will remain in the open set $z_1 \in (-k_a, k_b)$, $\forall t \in [0, +\infty)$ if the following inequality holds:

$$\dot{V} = \frac{\partial V}{\partial z}h \le -\rho V + C$$

where ρ and C are positive constants.

As shown in Fig. 2, $x = -k_a$ and $x = k_b$ are left and right boundary lines of an ABLF, respectively, and $k_a \ne k_b$, $k_a > 0$, and $k_b > 0$.

Lemma 2: The following inequality holds for $x \in \mathbf{R}$ in interval $|x| < k_a$, for any positive constant $k_a \in \mathbf{R}$:

$$\frac{k_a^2}{\pi}\cot\left(\frac{\pi}{2} - \frac{\pi}{2}\frac{x^2}{k_a^2}\right) \le x^2\csc^2\left(\frac{\pi}{2} - \frac{\pi}{2}\frac{x^2}{k_a^2}\right).$$

Proof: Define

$$g(x) = x^2\csc^2\left(\frac{\pi}{2} - \frac{\pi}{2}\frac{x^2}{k_a^2}\right) - \frac{k_a^2}{\pi}\cot\left(\frac{\pi}{2} - \frac{\pi}{2}\frac{x^2}{k_a^2}\right).$$

Since $g'(x) > 0$ when $x \in [-k_a, 0)\bigcup(0, k_a]$, $g'(0) = 0$ and $g(0) = 0$, we have $g(x) \ge 0$ in the interval $|x| < k_a$. ■

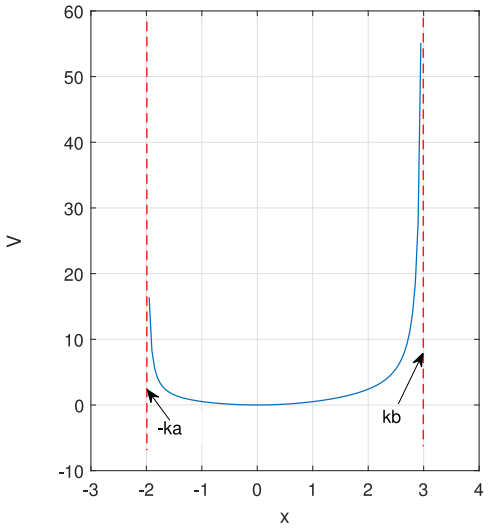

Fig. 2. ABLF.

The dynamics of the exoskeleton robot can be described by

$$\dot{\mathbf{x}}_r = J(q)\dot{q} \tag{21}$$

$$M(q)\ddot{q} + C(q,\dot{q})\dot{q} + F(\dot{q}) + G(q) = \tau + \tau_{\text{int}} \tag{22}$$

where $J(q)$ is assumed to be nonsingular.

Property 1: The matrix $\dot{M}(q) - 2C(q,\dot{q})$ is skew-symmetric.

We rewrite (21) and (22) by defining $x_1 = \mathbf{x}_r$, $x_2 = \dot{q}$

$$\dot{x}_1 = J\left(f^{-1}(x_1)\right)x_2 \tag{23}$$

$$\dot{x}_2 = M^{-1}\left(f^{-1}(x_1)\right)\Big[\tau + \tau_{\text{int}} - C\left(f^{-1}(x_1), x_2\right)x_2 - F(x_2) - G\left(f^{-1}(x_1)\right)\Big]. \tag{24}$$

The control purpose is to design a controller for the robot to enable it to follow a desired trajectory $x_d(t) = [x_{d1}(t), x_{d2}(t), \ldots, x_{dm}(t)]^T$ with all signals bounded and their own constraints not violated.

Assumption 1: There exist positive m-dimensional constant vectors $\underline{Y}_0 = [\underline{y}_{01}, \underline{y}_{02}, \ldots, \underline{y}_{0m}]^T$, $\overline{Y}_0 = [\overline{y}_{01}, \overline{y}_{02}, \ldots, \overline{y}_{0m}]^T$ and $A_0 = [a_{01}, a_{02}, \ldots, a_{0m}]^T$, satisfying $\max\{\underline{Y}_0, \overline{Y}_0\} \le A_0 \le k_c$, such that the desired trajectory $x_d(t)$ satisfies $-\underline{Y}_0 \le x_d(t) \le \overline{Y}_0$, $\forall t \ge 0$.

Let $z_1 = [z_{11}, z_{12}, \ldots, z_{1m}]^T = x_1 - x_d$ and $z_2 = [z_{21}, z_{22}, \ldots, z_{2n}]^T = x_2 - \alpha$, where $\alpha = [\alpha_1, \alpha_2, \ldots, \alpha_n]^T$ is a stabilizing function to be designed.

Choose the ABLF as

$$V_1 = \sum_{i=1}^{m}\left(p(i)\frac{k_{bi}^2}{\pi}\cot\left(\frac{\pi}{2} - \frac{\pi}{2}\frac{z_{1i}^2}{k_{bi}^2}\right) + (1-p(i))\frac{k_{ai}^2}{\pi}\cot\left(\frac{\pi}{2} - \frac{\pi}{2}\frac{z_{1i}^2}{k_{ai}^2}\right)\right) \tag{25}$$

where $k_a = [k_{a1}, k_{a2}, \ldots, k_{am}]^T = k_c - \underline{Y}_0$, $k_b = [k_{b1}, k_{b2}, \ldots, k_{bm}]^T = k_c - \overline{Y}_0$. $p(i)$ is defined as

$$p(i) = \begin{cases} 1, & z_{1i} > 0 \\ 0, & z_{1i} < 0 \end{cases} \quad i = 1, 2, \ldots, m. \tag{26}$$

The differential of V_1 with respect to time is

$$\dot{V}_1 = \sum_{i=1}^{m}\left(p(i)\csc^2\left(\frac{\pi}{2} - \frac{\pi}{2}\frac{z_{1i}^2}{k_{bi}^2}\right)z_{1i}\dot{z}_{1i} + (1-p(i))\csc^2\left(\frac{\pi}{2} - \frac{\pi}{2}\frac{z_{1i}^2}{k_{ai}^2}\right)z_{1i}\dot{z}_{1i}\right). \tag{27}$$

Differentiating z_1 with respect to time yields

$$\dot{z}_{1i} = \dot{x}_{1i} - \dot{x}_{di} = J_i(z_2 + \alpha) - \dot{x}_{di} \tag{28}$$

where J_i is the ith row of $J(f^{-1}(x_1))$. The stabilizing function α is designed as

$$\alpha = J^{+}(\dot{x}_d - A_1) \tag{29}$$

where the ith element of A_1 is defined as

$$A_{1i} = \left(p(i)\sin^2\left(\frac{\pi}{2} - \frac{\pi}{2}\frac{z_{1i}^2}{k_{bi}^2}\right) + (1-p(i))\sin^2\left(\frac{\pi}{2} - \frac{\pi}{2}\frac{z_{1i}^2}{k_{ai}^2}\right)\right)k_i z_{1i} \tag{30}$$

where k_i, $i = 1, 2, \ldots, m$, are positive constants, and J^{+} is the Moore–Penrose pseudo-inverse of J, that is, $J^{+} = J^T(JJ^T)^{-1}$. Substituting (29) into (28), we have

$$\dot{z}_1 = Jz_2 - A_1$$

and substituting the above equation and (30) into (27), we have

$$\dot{V}_1 = -\sum_{i=1}^{m}k_i z_{1i}^2 + \sum_{i=1}^{m}\left(p(i)\csc^2\left(\frac{\pi}{2} - \frac{\pi}{2}\frac{z_{1i}^2}{k_{bi}^2}\right)z_{1i}J_i z_2 + (1-p(i))\csc^2\left(\frac{\pi}{2} - \frac{\pi}{2}\frac{z_{1i}^2}{k_{ai}^2}\right)z_{1i}J_i z_2\right). \tag{31}$$

Choose the Lyapunov function V_2 as

$$V_2 = V_1 + \frac{1}{2}z_2^T M z_2. \tag{32}$$

Differentiating V_2 with respect to time yields

$$\dot{V}_2 = \dot{V}_1 + z_2^T M\dot{z}_2 + \frac{1}{2}z_2^T\dot{M}z_2. \tag{33}$$

The differential of z_2 with respect to time is

$$\dot{z}_2 = \dot{x}_2 - \dot{\alpha} = M^{-1}\left(f^{-1}(x_1)\right)\Big[\tau + \tau_{\text{int}} - C\left(f^{-1}(x_1), x_2\right)x_2 - F(x_2) - G\left(f^{-1}(x_1)\right)\Big] - \dot{\alpha}. \tag{34}$$

Substituting (31) and (34) into (33), and applying Property 1, we have

$$\dot{V}_2 = -\sum_{i=1}^{m}k_i z_{1i}^2 + \sum_{i=1}^{m}\left(p(i)\csc^2\left(\frac{\pi}{2} - \frac{\pi}{2}\frac{z_{1i}^2}{k_{bi}^2}\right)z_{1i}J_i z_2 + (1-p(i))\csc^2\left(\frac{\pi}{2} - \frac{\pi}{2}\frac{z_{1i}^2}{k_{ai}^2}\right)z_{1i}J_i z_2\right) + z_2^T(\tau + \tau_{\text{int}} - C\alpha - G - F - M\dot{\alpha}). \tag{35}$$

The parameters of the robot system $M(f^{-1}(x_1))$, $C(f^{-1}(x_1), x_2)$, $F(x_2)$, and $G(f^{-1}(x_1))$ may be unknown or inaccurate in practice, and it may be unfeasible to design a model-based control law. To solve this issue, we use an adaptive NN to approximate the unknown parameters. The control law is designed as follows:

$$\begin{aligned}\tau = &-\sum_{i=1}^{m}\left(p(i)\csc^2\left(\frac{\pi}{2}-\frac{\pi}{2}\frac{z_{1i}^2}{k_{bi}^2}\right)z_{1i}J_i^T\right.\\&\left.+(1-p(i))\csc^2\left(\frac{\pi}{2}-\frac{\pi}{2}\frac{z_{1i}^2}{k_{ai}^2}\right)z_{1i}J_i^T\right)\\&-\sum_{i=1}^{m}\left(p(i)\csc^2\left(\frac{\pi}{2}-\frac{\pi}{2}\frac{z_{1i}^2}{k_{bi}^2}\right)k_i z_{1i}^2\left(z_2^T\right)^+\right.\\&\left.+(1-p(i))\csc^2\left(\frac{\pi}{2}-\frac{\pi}{2}\frac{z_{1i}^2}{k_{ai}^2}\right)k_i z_{1i}^2\left(z_2^T\right)^+\right)\\&-K_2 z_2-\hat{W}^T S(Z)-\tau_{\text{int}}\end{aligned}\tag{36}$$

where K_2 is an $n\times n$ positive definite matrix, $(z_2^T)^+$ is the Moore–Penrose pseudo-inverse of z_2^T, $\hat{W}=[\hat{W}_1,\hat{W}_2,\ldots,\hat{W}_n]$ are the estimated weights of the NN, $S(Z)$ are the basis functions of the NN, and $Z=[x_1^T,x_2^T,\alpha^T,\dot{\alpha}^T]^T$ is the inputs of the NN. The dynamics of the robot is approximated by the NN $\hat{W}^T S(Z)$ as

$$\begin{aligned}W^{*T}S(Z)=&-\Big(C\Big(f^{-1}(x_1),x_2\Big)\alpha+G\Big(f^{-1}(x_1)\Big)+F(x_2)\\&+M\Big(f^{-1}(x_1)\Big)\dot{\alpha}\Big)-\epsilon(Z)\end{aligned}\tag{37}$$

where $\epsilon(Z)\in\mathbf{R}^n$ is the error of approximation and W^* is the actual value of the NN weight. The adaptive law of the NN is designed as follows:

$$\dot{\hat{W}}_i=\Gamma_i\Big[S(Z)z_{2i}-\sigma_i|z_{2i}|\hat{W}_i\Big],\ i=1,2,\ldots,n\tag{38}$$

where $\Gamma_i=\Gamma_i^T>0$, $i=1,2,\ldots,n$ are constant gain matrices, and $\sigma_i>0$, $i=1,2,\ldots,n$ are small constants [31].

Lemma 3 [32]: For the adaptive law (38), there exists a compact set

$$\Omega_{\omega 1}=\left\{\hat{W}_i\middle|\left\|\hat{W}_i\right\|\le\frac{s}{\sigma_i}\right\}$$

where $\|S(Z)\|\le s$ with $s>0$, such that $\hat{W}_i(t)\in\Omega_{\omega 1}$, $\forall t\ge 0$ provided that $\hat{W}_i(0)\in\Omega_{\omega 1}$.

Theorem 1: Consider the robot system described in (23) and (24), under Assumption 1, with control law (36) and adaptation law (38), for initial conditions satisfying $z_1(0)\in\Omega_0:=z_1\in\mathbf{R}^2:-k_a<z_1<k_b$. Then, all signals of the robot system are semiglobally uniformly bounded (SGUB) as well as asymptotic tracking achieved, that is, $x_1(t)\to x_d(t)$ as $t\to\infty$. Therefore, the multiple output constraints are never violated, that is, $|x_1|<k_c$, $\forall t>0$, and the error signals of the system z_1, z_2, and $\tilde{W}$ will remain within the compact sets Ω_{z_1}, Ω_{z_2}, and $\Omega_{\tilde{W}}$, respectively, defined by

$$\Omega_{z_1}=\left\{z_1\in\mathbf{R}^2\mid -\underline{D}_{z_{1i}}\le z_{1i}\le\overline{D}_{z_{1i}},i=1,2\right\}\tag{39}$$

$$\Omega_{z_2}=\left\{z_2\in\mathbf{R}^2\mid\|z_2\|\le\sqrt{\frac{D}{\lambda_{\min}(M)}}\right\}\tag{40}$$

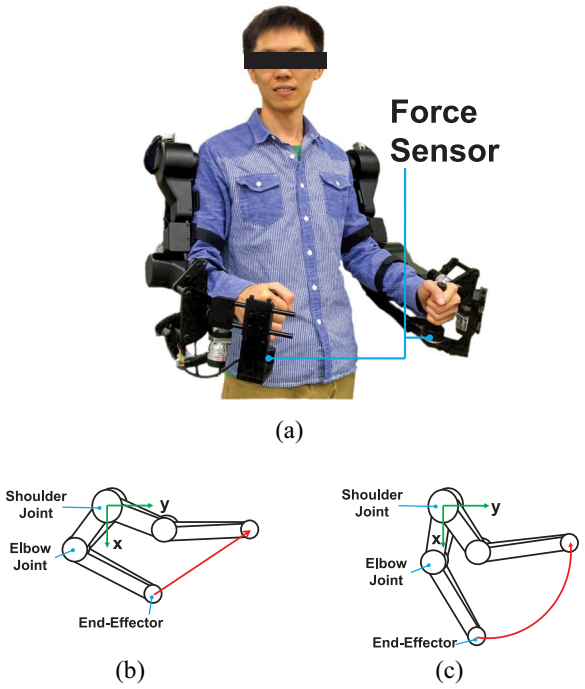

Fig. 3. (a) Developed dual-arm exoskeleton. Illustration of (b) experiment 1 and (c) experiment 2.

where

$$\underline{D}_{z_{1i}}=\sqrt{k_{ai}^2\left(1-\frac{2}{\pi}\operatorname{arccot}\left(\frac{\pi\left(V_2(0)+\frac{C}{\rho}\right)}{k_{ai}^2}\right)\right)}$$

$$\overline{D}_{z_{1i}}=\sqrt{k_{bi}^2\left(1-\frac{2}{\pi}\operatorname{arccot}\left(\frac{\pi\left(V_2(0)+\frac{C}{\rho}\right)}{k_{bi}^2}\right)\right)}$$

$$D=2(V_2(0)+C/\rho)$$

and ρ and C are two positive constants.

III. Experiments on the Robotic Exoskeleton

A. Experimental Description

The dual-arm exoskeleton robot developed in the SCUT laboratory for experiments consists of two 6-DOF exoskeleton arms, as shown in Fig. 3(a). Each arm has two shoulder abduction/adduction joints, a shoulder rotation joint, an elbow joint, and tow wrist joints. The kinematical chain is similar to the upper limb of the human. Each joint contains a high-resolution encoder (2048 pulse/cycle) and a Hall effect sensor used for position sensing and measurements. The robotic exoskeleton is developed using dc motors as actuators, and the Maxon dc flat brushless motor EC45 is chosen as the driver unit. Only the right arm's shoulder and elbow joint are used in the experiments. The force sensor is used to measure the interaction force between the human and dual-arm exoskeleton robot, which is mounted on the end-effector.

Two different tasks involving the motion of drawing specific lines by the human hand in the $x-y$ plane are presented, as illustrated in Fig. 3(b) and (c), with the green line representing the coordinate frame of the $x-y$ plane and the red line

TABLE II
INFORMATION OF THE EXPERIMENTER

Experimenter	Age	Weight	Height
Demonstrator	28	60.5 kg	173 cm
Subject. 1	23	62.5 kg	175 cm
Subject. 2	23	72.1 kg	180 cm

representing the motion trajectories of the end-effector. During the demonstration, for teaching the robot, the human hand should display a minimum required impedance. The demonstrator grasps the force sensor which is attached to the end-effector of the exoskeleton robot, and draws a line in the $x-y$ plane. The robot receives force feedback information from the force sensor and applied admittance controller to generate the desired position of the end-effector in task space, which is the input of the ABLF-based adaptive NN controller to be tracked. In the reproduction phase, where a subject tries to drive the end-effector to fulfill the task, the forces different from demonstrations are exerted, and the GMR model is applied to predict the expected interaction force, and further to calculate the assistive force that the robot should produce to aid the human by using the PID force control scheme. Table II shows relevant information of one demonstrator and two subjects.

The desired damping and stiffness matrices of the mass–spring–damper system are chosen to be $\Psi = 60I$ and $\Gamma = 100I$, respectively, and the number of Gaussians in GMM is chosen to be 3. For the admittance controller, the desired virtual inertia $\mathbf{M}_d$ and virtual damping $\mathbf{C}_d$ are chosen as $2I$ and $24I$, respectively. These parameters are chosen empirically. As for the ABLF-based adaptive NN controller, we choose 2^8 nodes for model approximation, and the centers are evenly distributed in: $[-0.5, 0.5] \times [-0.5, 0.5] \times [-0.5, 0.5] \times [-0.5, 0.5] \times [-0.5, 0.5] \times [-0.5, 0.5] \times [-0.5, 0.5] \times [-0.5, 0.5]$ with each parameter either being -0.5 or 0.5. We choose the control gains K_1, K_2, as $K_1 = \text{diag}[k_1, k_2] = \text{diag}[15.5, 19.5]$, $K_2 = \text{diag}[2.0, 2.1]$, $\Gamma_1 = I$, $\Gamma_2 = I$, $\sigma_1 = 0.2$, and $\sigma_2 = 0.2$.

B. Experiment 1: Drawing a Straight Line

During the demonstration, as can be seen in Fig. 3(b), the demonstrator needs to guide the robot end-effector to draw a straight line successfully in the $x-y$ plane. There are a total of 25 successful trials, each lasting for around 10 s when recorded, and the data recording rate is 25 Hz which results in around 250 sample points for each trial. Fig. 4 shows the experimental results of one of the demonstrations in the experiment 1.

In the reproduction phase, two different subjects participated in the same task. The results are shown in Figs. 5 and 6. The trajectories of the end-effector in the $x-y$ plane are shown in Figs. 4(c), 5(c), and 6(c). The input torques of joints are shown in Figs. 4(d), 5(d), and 6(d). Figs. 4(a), 5(a), and 6(a) illustrate the tracking trajectories and the desired trajectories, and the tracking error z_1 is shown in Figs. 4(b), 5(b), and 6(b). We can see that both x_1 and z_1 are within the predefined set, thus asymptotic tracking has been achieved. Figs. 5(e), 5(f), 6(e), and 6(f) show the interaction force

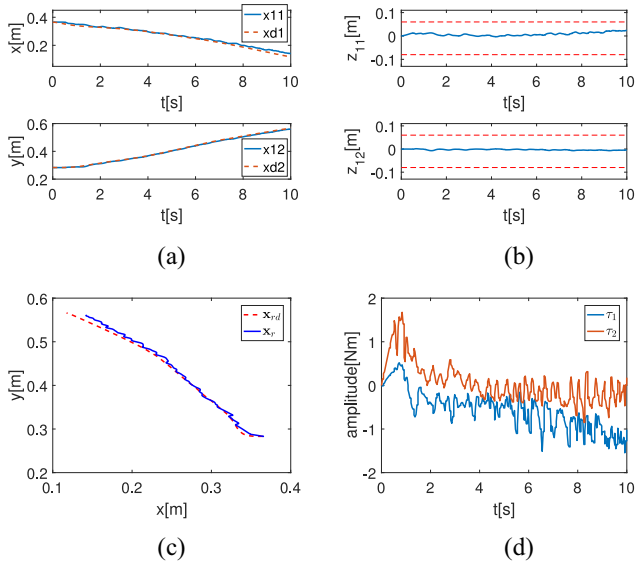

Fig. 4. Experimental results of one of the demonstrators in experiment 1. (a) Tracking trajectory. (b) Tracking error. (c) Trajectory in the $x-y$ plane. (d) Input torques of the joints.

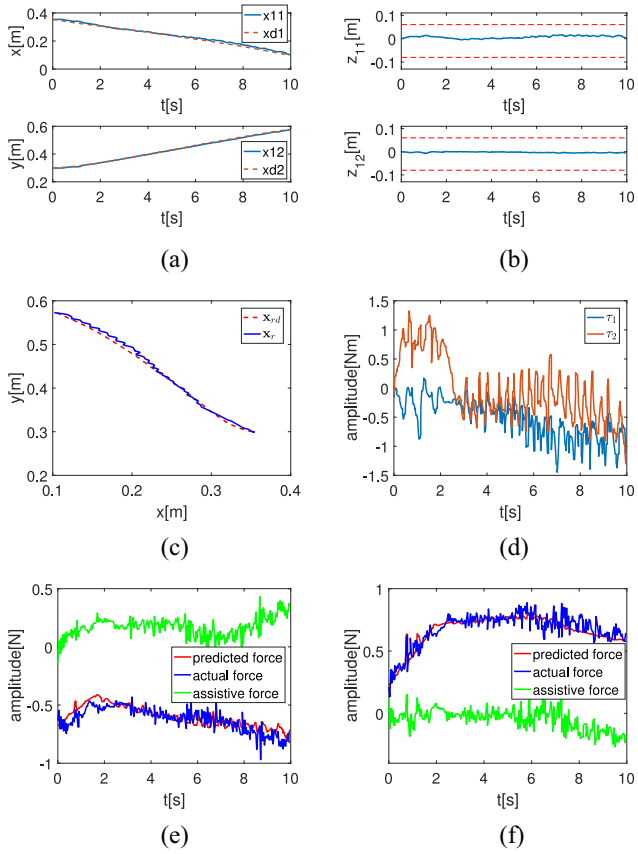

Fig. 5. Experimental results of subject 1 in the experiment 1. (a) Tracking trajectory. (b) Tracking error. (c) Trajectory in the $x-y$ plane. (d) Input torques of the joints. (e) Force in the x direction. (f) Force in the y direction.

information during reproduction in the x and y direction, respectively, and we can see that when the actual interaction force (the blue line) deviates from the predicted one (the red line), which is obtained by (13), the exoskeleton robot provides just enough assistive force (the green line) calculated by

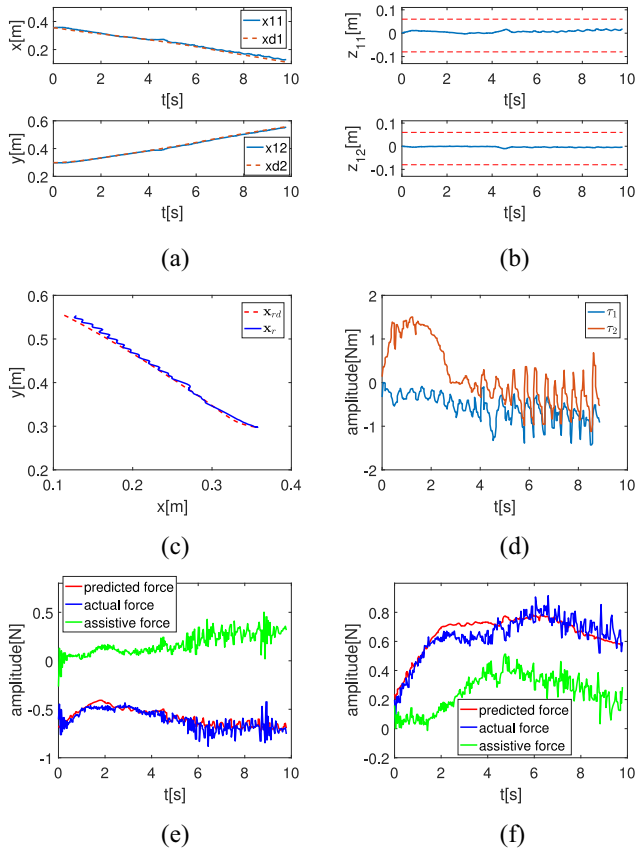

Fig. 6. Experimental results of subject 2 in the experiment 1. (a) Tracking trajectory. (b) Tracking error. (c) Trajectory in the $x-y$ plane. (d) Input torques of the joints. (e) Force in the x direction. (f) Force in the y direction.

the proposed force control scheme in (20) to aid the subjects to complete the task.

Fig. 10(a) shows trajectories of the end-effector reproduced by subjects (the blue and green lines), and we can see that with the assistance of the robot (the solid lines), the motion remains in the zone where the task can be fulfilled successfully, but without the assistance (the dotted lines), the subjects could not push forward far enough to fulfill the task.

C. Experiment 2: Drawing Curve

To verify the effectiveness of the proposed control scheme in different motions of human–robot cooperative manipulation, a task of drawing a curve in the $x-y$ plane is presented in experiment 2, as illustrated in Fig. 3(c). There are also 25 successful trials, each lasting for around 10 s when recorded, and the data recording rate is the same as experiment 1, which results in around 250 sample points for each trial. Fig. 7 shows the experimental results of one of the demonstrations in experiment 2.

In the reproduction phase, two different subjects tried to perform a similar motion as the one in the demonstration phase. The results are shown in Figs. 8 and 9. The trajectories of the robot end-effector in the $x-y$ plane are shown in Figs. 7(c), 8(c), and 9(c). The input torques of the joints are shown in Figs. 7(d), 8(d), and 9(d). Figs. 7(a), 8(a), and 9(a) are the tracking trajectories, and tracking errors z_1 are shown in

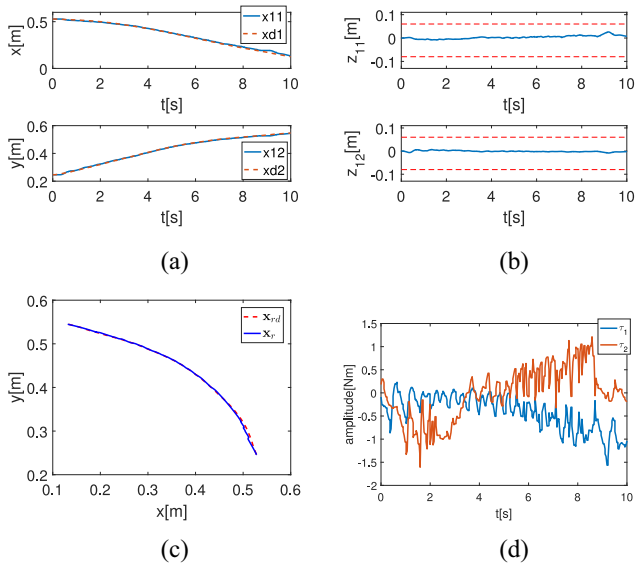

Fig. 7. Experimental results of one of the demonstrator in the experiment 2. (a) Tracking trajectory. (b) Tracking error. (c) Trajectory in $x-y$ plane. (d) Input torques of the joints.

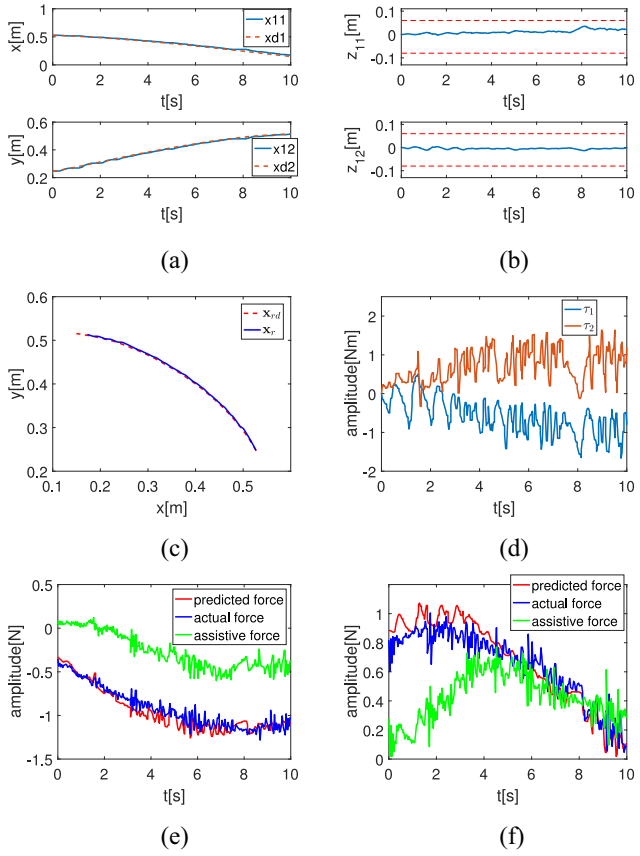

Fig. 8. Experimental results of the subject 1 in experiment 2. (a) Tracking trajectory. (b) Tracking error. (c) Trajectory in $x-y$ plane. (d) Input torques of the joints. (e) Force in the x direction. (e) Force in the y direction.

Figs. 7(b), 8(b), and 9(b). We can see that asymptotic tracking is also achieved in experiment 2. Figs. 8(e), 8(f), 9(e), and 9(f) show the interaction force information during reproduction in the x and y direction, respectively, and the results are similar

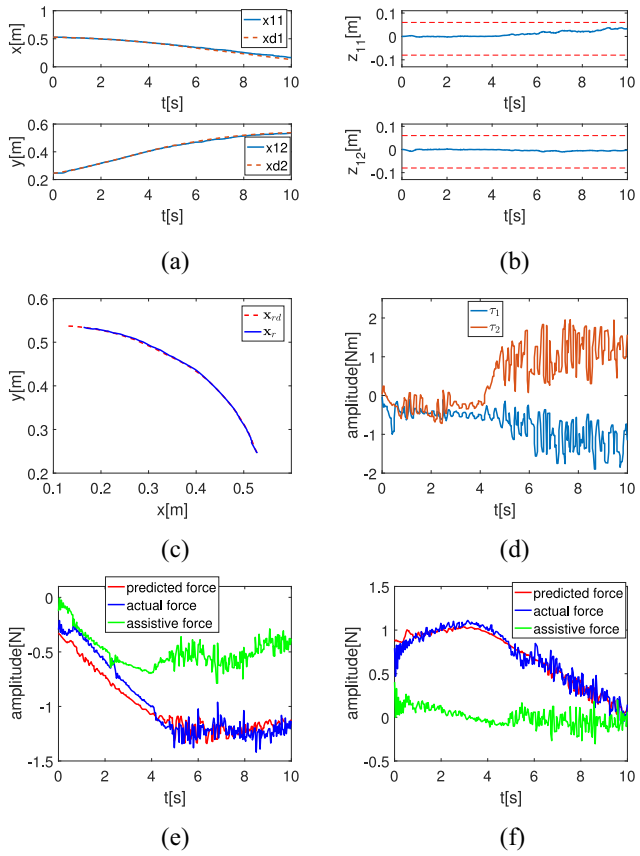

Fig. 9. Experimental results of subject 2 in the experiment 2. (a) Tracking trajectory. (b) Tracking error. (c) Trajectory in the $x-y$ plane. (d) Input torques of the joints. (e) Force in the x direction. (f) Force in the y direction.

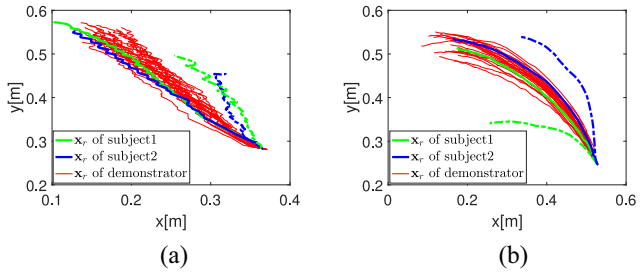

Fig. 10. Trajectories of the robot end-effector. The green and blue solid lines are trajectories of the subjects with the assistive force of the robot, and the dotted lines are without the assistive force. (a) Trajectories in experiment 1. (b) Trajectories in experiment 2.

to that in the experiment 1. As can be seen, the assistance is provided only when needed by the robot, that is, the assistive force (the green line) remains zero when the subjects actively push the robot end-effector, and increases when the subjects get tired or the task difficulty increases.

Fig. 10(b) shows that trajectories of the end-effector were reproduced by the subjects (the blue and green lines) in experiment 2, and we can also see that the subjects successfully performed the task with the assistance of the robot (the solid lines) but failed without the assistance (the solid lines) and the motion deviated far from the desired ones.

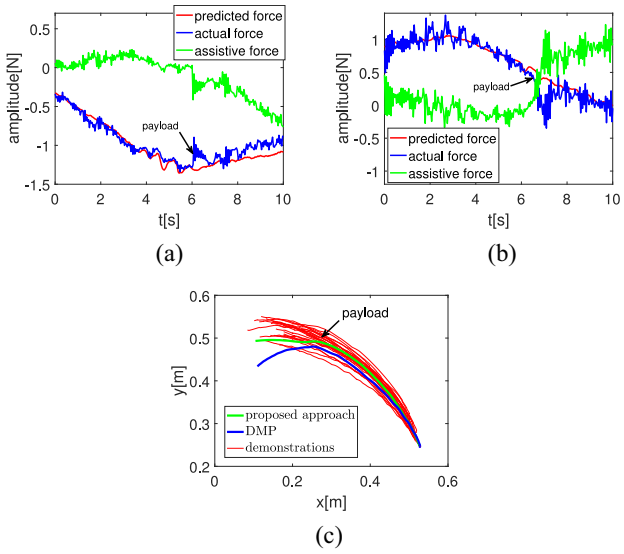

Fig. 11. Experimental results of the experiment with an unknown payload exerted at about $t = 6$ s. (a) and (b) Force results of the proposed approach. (c) Trajectories results in the $x - y$ plane, and the blue line is trajectory generated using DMP and the green line is generated using the proposed approach.

D. Robustness to Variation Due to Disturbances

In order to show that the proposed approach is robust to variation in the interaction force caused by payload exerted during reproduction, the demonstrator is supposed to execute the task in experiment 2, and an unmodeled, random, and unknown payload is exerted on his hand at about $t = 6$ s during task execution. The task is executed twice in this case. First, the task is executed using the DMP presented in [10]. The DMP for the task has 2 dimensions to represent the position of the end-effector in the $x - y$ plane, and the parameters of the DMP are trained through supervised learning with a dataset recorded during demonstration. Then, the desired position of the end-effector is retrieved using the trained DMP during reproduction. As the demonstrator was performing the task, the payload was exerted on his hand and the motion deviated far from the desired, and the result is shown in Fig. 11(c) with the blue line. The second time is executed with the proposed control scheme. When the payload was exerted on the human hand to change the interaction force, the robot provided the demonstrator with assistance to compensate for the difference between the actual interaction force and the predicted force, such that the task was completed successfully. Fig. 11 shows the results in the case. From Fig. 11(c), we can see that when the disturbance is exerted, the trajectory generated using DMP deviates from the desired one as in demonstrations, which is shown in the blue line, but remains in the area where the task can be completed successfully if the trajectory is generated using the proposed approach, which is shown in the green line. And from Fig. 11(a) and (b), we can see that the assistive force is close to zero at the beginning but increases after the payload is exerted, which shows the resilience of the proposed approach to such a disturbance.

E. Converge to New Targets

The task-parameterized GMM presented in Section II-B is trained with a dataset collected in experiment 2, and the

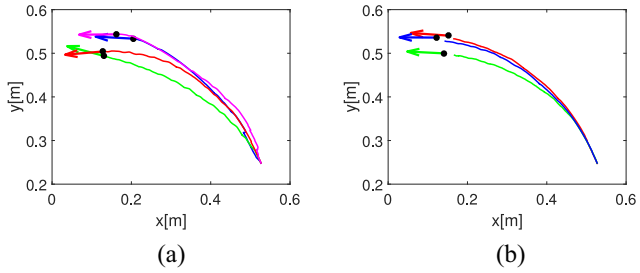

Fig. 12. Trajectories of demonstration and reproduction performing the same task, but with different targets. Targets of each trajectory are plotted with black points (position) and arrows (orientation) in the same color as corresponding trajectories.

reproduction experiments are performed by subject 1 with new targets different from those of demonstrations. Fig. 12 presents the demonstration and reproduction results. Targets of each trajectory are plotted with black points, and the orientation of each target is plotted with an arrow in the same color as its corresponding trajectory. Only 4 of 25 demonstrations are shown in Fig. 12(a), and three reproduction trials with new different targets are shown in Fig. 12(b). We can see from Fig. 12(b) that all three trials converge to new targets with minor errors, which show the extrapolation capability of task-parameterized GMM, that is, its adaptation ability to new situations.

IV. Discussion

We have made comparisons with related literature in the field in two aspects. The first one is that the variability of human–robot cooperative manipulation among multiple demonstrations should be considered and exploited in the reproduction phase. From the experiment results shown in Figs. 6(e), 8(e), 9(e), and 11, we can see that there exist differences between the predicted force and the actual, since the variability information among demonstrations encoded in GMM is retrieved by GMR and calculated by (12), and then it is used in the PID force controller to adaptively regulate K, I, and D such that the error $E(t)$ is allowed but would not be large, and the assistance is provided only when needed. The second one is that the physical constraints of the upper limb exoskeleton should be considered, and ABLF has an advantage over BLF when dealing with asymmetric constraints. Experimental results in Figs. 4(b), 5(b), 6(b), 7(b), 8(b), and 9(b) show that the tracking error curve is between the upper dashed line ($k_b = 0.06$) and the lower dashed line ($-ka = -0.08$). It is achieved with the use of ABLF in the motion control of the robot. ABLF enables the user to define the lower and upper output constraint by tuning k_a and k_b such that the output constraint in the task space ($-k_a + \underline{Y}_0 \leq \mathbf{x}_r \leq k_b + \overline{Y}_0$) is never violated, and asymptotic tracking without violating asymmetric output constraints is achieved, while the BLF cannot.

Upper limbs of robot-assisted rehabilitation could be a target application of the proposed method, and the benefits can be evaluated from three aspects. It reduces the workload of the therapists. The learning model enables the robot to learn how to aid the subjects from demonstrations, and it does not require any programming of the robot by the therapists which can be cumbersome, or the modeling of human–robot interaction which is considered to be tedious. It can provide different training tasks which can enhance motor function recovery of the subjects, without reprogramming the robot but just by showing the robot how to fulfill these tasks successfully with demonstrations. It can be applied to subjects with different degrees of injury, since the robot can adjust the assistive force according to the difference between the current interaction force and the ones in the demonstrations, to help the subjects fulfill the training tasks successfully.

V. Conclusion

In this paper, a hierarchical control scheme, that is, a high-level statistical model for interaction which can transfer human experience and skills to the robot by learning and a low-level robot motion control that enable robots to be back drivable, has been proposed for human–robot co-manipulation. The proposed high-level Gaussian mixture framework and the low-level admittance control with a newly designed ABLF-based adaptive NN controller can achieve safe human–robot cooperative manipulation in impedance-based tasks. The validity of the proposed approach has been verified by using experiments involving two different kinds of human–robot cooperative manipulations.

Appendix
Proof of Theorem 1

Considering the Lyapunov function V_2 as

$$V_2 = V_1 + \frac{1}{2} z_2^T M z_2 + \frac{1}{2} \sum_{i=1}^{n} \tilde{W}_i^T \Gamma_i^{-1} \tilde{W}_i \tag{41}$$

where $\tilde{W}_i = \hat{W}_i - W_i^*$, $(i = 1, 2, \ldots, n)$ is the weight error of the NN. Differentiating V_2 with respect to time and considering (35)–(38), we have

$$\begin{aligned}\dot{V}_2 = &- \sum_{i=1}^{m} \left(p(i) \csc^2 \left(\frac{\pi}{2} - \frac{\pi}{2} \frac{z_{1i}^2}{k_{bi}^2} \right) k_i z_{1i}^2 z_2^T \left(z_2^T\right)^+ \right. \\ &\left. + (1 - p(i)) \csc^2 \left(\frac{\pi}{2} - \frac{\pi}{2} \frac{z_{1i}^2}{k_{ai}^2} \right) k_i z_{1i}^2 z_2^T \left(z_2^T\right)^+ \right) \\ &+ z_2^T \left(-\hat{W}^T S(Z) + W^{*T} S(Z) + \epsilon(Z) \right) - z_2^T K_2 z_2 \\ &- \sum_{i=1}^{m} k_i z_{1i}^2 + \sum_{i=1}^{n} \tilde{W}_i^T \left[S(Z) z_{2i} - \sigma_i |z_{2i}| \hat{W}_i \right]. \end{aligned} \tag{42}$$

According to definition of the Moore–Penrose pseudo-inverse, we have

$$z_2^T \left(z_2^T\right)^+ = \begin{cases} 0, & z_2 = [0, \ldots, 0]^T \\ 1, & z_2 \neq [0, \ldots, 0]^T. \end{cases} \tag{43}$$

If $z_2 = [0, \ldots, 0]^T$, $V_2 = -\sum_{i=1}^{m} k_i z_{1i}^2 \leq 0$, then according to Barbalat's lemma, asymptotic stability of the system can be

achieved. Otherwise, it is easy to obtain

$$z_2^T\left(-\hat{W}^T S(Z)+W^{*T}S(Z)\right)+\sum_{i=1}^{n}\tilde{W}_i^T S(Z)z_{2i}=0$$
$$z_2^T\epsilon(Z)\le\frac{1}{2}z_2^Tz_2+\frac{1}{2}\|\epsilon(Z)\|^2$$
$$-W_i^{*T}\tilde{W}_i\le\frac{1}{2}\left(\|\tilde{W}_i\|^2+\|W_i^*\|^2\right)$$
$$-\sum_{i=1}^{n}|z_{2i}|\frac{\sigma_i}{2}\left(\|\tilde{W}_i\|^2-\|W_i^*\|^2\right)\le\frac{1}{2}z_2^Tz_2+\sum_{i=1}^{n}\frac{\sigma_i^2}{8}\left(\|\tilde{W}_i\|^4+\|W_i^*\|^4-2\tilde{W}_i\|^2\|W_i^*\|^2\right).$$

Considering the above equations and by applying Lemma 2 to (43), we have

$$\dot{V}_2\le-z_2^T(K_2-I)z_2+\frac{1}{2}\|\epsilon(Z)\|^2+\sum_{i=1}^{n}\frac{\sigma_i^2}{8}\left(\|\tilde{W}_i\|^4+\|W_i^*\|^4-2\tilde{W}_i\|^2\|W_i^*\|^2\right)-\sum_{i=1}^{m}k_i\left(p(i)\frac{k_{bi}^2}{\pi}\cot\left(\frac{\pi}{2}-\frac{\pi}{2}\frac{z_{1i}^2}{k_{bi}^2}\right)+(1-p(i))\frac{k_{ai}^2}{\pi}\cot\left(\frac{\pi}{2}-\frac{\pi}{2}\frac{z_{1i}^2}{k_{ai}^2}\right)\right).\quad(44)$$

According to Lemma 3, we have

$$\|\tilde{W}_i\|=\|\hat{W}_i-W_i^*\|\le\|\hat{W}_i\|+\|W_i^*\|\le\frac{s}{\sigma_i}+\|W_i^*\|.\quad(45)$$

For clarification, we can define

$$\|\tilde{W}_i\|\le\frac{s}{\sigma_i}+\|W_i^*\|=\vartheta\quad(46)$$

where ϑ is a positive constant. Further, we have

$$\dot{V}_2\le-z_2^T(K_2-I)z_2+\frac{1}{2}\|\epsilon(Z)\|^2+\sum_{i=1}^{n}\frac{\sigma_i^2}{8}\left(\vartheta^4+\|W_i^*\|^4-2\tilde{W}_i\|^2\|W_i^*\|^2\right)-\sum_{i=1}^{m}k_i\left(p(i)\frac{k_{bi}^2}{\pi}\cot\left(\frac{\pi}{2}-\frac{\pi}{2}\frac{z_{1i}^2}{k_{bi}^2}\right)+(1-p(i))\frac{k_{ai}^2}{\pi}\cot\left(\frac{\pi}{2}-\frac{\pi}{2}\frac{z_{1i}^2}{k_{ai}^2}\right)\right).\quad(47)$$

Compare the right side of (47) and $-\rho V_2+C$, and choose ρ and C to be

$$\rho=\min\left(\min(k_i),\frac{2\lambda_{\min}(K_2-I)}{\lambda_{\max}(M)}\min\left(\frac{\sigma_i^2\|W_i^*\|^2}{2\lambda_{\max}\left(\Gamma_i^{-1}\right)}\right)\right)\quad(48)$$

$$C=\frac{1}{2}\|\bar{\epsilon}\|^2+\sum_{i=1}^{n}\frac{\sigma_i^2}{8}\left(\vartheta^4+\|W_i^*\|^4\right)\quad(49)$$

where $\lambda_{\min}(B)$ and $\lambda_{\max}(B)$ are the minimum and maximum eigenvalues of matrix B, respectively. We choose the control gain K_2 satisfying the following condition such that $\rho>0$:

$$\lambda_{\min}(K_2-I)>0.\quad(50)$$

Then we have

$$\dot{V}_2\le-\rho V_2+C.\quad(51)$$

From Lemma 1, the tracking error $z_1(t)$ remains in the set $z_1\in(-k_a,k_b)$, $\forall t\in[0,+\infty)$, provided that $z_1(0)\in(-k_a,k_b)$. Since $x_1(t)=z_1(t)+x_d(t)$, $-\underline{Y}_0\le x_d(t)\le\overline{Y}_0$, and $k_a=k_c-\underline{Y}_0$, $k_b=k_c-\overline{Y}_0$, the output constraints are not violated, that is, $|x_1|\le k_c$, $\forall t\ge0$.

To prove that the signals $z_1,z_2,\tilde{W}_i(i=1,2,\ldots,n)$ are SGUB, we multiply (51) by $e^{\rho t}$ and have

$$\frac{d}{dt}\left(V_2e^{\rho t}\right)\le Ce^{\rho t}.\quad(52)$$

Integrating (52) over $[0,t]$ leads to

$$V_2\le\left(V_2(0)-\frac{C}{\rho}\right)e^{-\rho t}+\frac{C}{\rho}\le V_2(0)+\frac{C}{\rho}.\quad(53)$$

According to (41) and (53), we have

$$\frac{1}{2}\|z_2\|^2\le\frac{V_2(0)+\frac{C}{\rho}}{\lambda_{\min}(M)}\quad(54)$$

and

$$V_2(0)+\frac{C}{\rho}\ge\begin{cases}\frac{k_{bi}^2}{\pi}\cot\left(\frac{\pi}{2}-\frac{\pi}{2}\frac{z_{1i}^2}{k_{bi}^2}\right) & 0<z_{1i}<k_{bi}\\ \frac{k_{ai}^2}{\pi}\cot\left(\frac{\pi}{2}-\frac{\pi}{2}\frac{z_{1i}^2}{k_{ai}^2}\right) & -k_{ai}<z_{1i}<0.\end{cases}\quad(55)$$

Considering the monotonicity of the inverse function of $\cot(\cdot)$, we have

$$z_{1i}^2\le\begin{cases}k_{bi}^2\left(1-\frac{2}{\pi}\operatorname{arccot}\left(\frac{\pi\left(V_2(0)+\frac{C}{\rho}\right)}{k_{bi}^2}\right)\right) & 0<z_{1i}<k_{bi}\\ k_{ai}^2\left(1-\frac{2}{\pi}\operatorname{arccot}\left(\frac{\pi\left(V_2(0)+\frac{C}{\rho}\right)}{k_{ai}^2}\right)\right) & -k_{ai}<z_{1i}<0.\end{cases}\quad(56)$$

Then, we have

$$-\underline{D}_{z_{1i}}\le z_{1i}\le\overline{D}_{z_{1i}}\quad(57)$$

where $\overline{D}_{z_{1i}}$ and $\underline{D}_{z_{1i}}$ are defined in Theorem 1.

REFERENCES

[1] M. Trlep, M. Mihelj, and M. Munih, "Skill transfer from symmetric and asymmetric bimanual training using a robotic system to single limb performance," *J. Neuroeng. Rehab.*, vol. 9, no. 43, pp. 1–14, 2012.

[2] T. S. Buchanan, D. G. Lloyd, K. Manal, and T. F. Besier, "Neuromusculoskeletal modeling: Estimation of muscle forces and joint moments and movements from measurements of neural command," *J. Appl. Biomech.*, vol. 20, no. 4, pp. 367–395, 2004.

[3] Z. Li *et al.*, "sEMG-based joint force control for an upper-limb power-assist exoskeleton robot," *IEEE J. Biomed. Health Inf.*, vol. 18, no. 3, pp. 1043–1050, May 2014.

[4] Z. Li *et al.*, "Asymmetric bimanual coordinate control of dual-arm exoskeleton robots for human cooperative manipulations," *IEEE Trans. Robot.*, vol. 34, no. 1, pp. 264–271, Feb. 2018.

[5] J. R. Medina, M. Lawitzky, A. Mörtl, D. Lee, and S. Hirche, "An experience-driven robotic assistant acquiring human knowledge to improve haptic cooperation," in *Proc. IEEE/RSJ Int. Conf. Intell. Robots Syst.*, 2011, pp. 2416–2422.

[6] D. Kulić, C. Ott, D. Lee, J. Ishikawa, and Y. Nakamura, "Incremental learning of full body motion primitives and their sequencing through human motion observation," *Int. J. Robot. Res.*, vol. 31, no. 3, pp. 330–345, 2011.

[7] R. Luo and D. Berenson, "A framework for unsupervised online human reaching motion recognition and early prediction," in *Proc. Int. Conf. Intell. Robots Syst.*, Hamburg, Germany, Sep. 2015, pp. 2426–2433.

[8] L. Rozo, S. Calinon, and D. G. Caldwell, "Learning force and position constraints in human–robot cooperative transportation," in *Proc. 23rd IEEE Int. Symp. Robot Human Interact. Commun.*, 2014, pp. 619–624.

[9] B. D. Argalla, S. Chernovab, M. Velosob, and B. Browning, "A survey of robot learning from demonstration," *Robot. Auton. Syst.*, vol. 57, no. 5, pp. 469–483, 2009.

[10] A. J. Ijspeert, J. Nakanishi, H. Hoffmann, P. Pastor, and S. Schaal, "Dynamical movement primitives: Learning attractor models for motor behaviors," *Neural Comput.*, vol. 25, no. 2, pp. 328–373, Feb. 2012.

[11] C.-A. Cheng, T.-H. Huang, and H.-P. Huang, "Bayesian human intention estimator for exoskeleton system," in *Proc. IEEE/ASME Int. Conf. Adv. Intell. Mechatronics*, Wollongong, NSW, Australia, 2013, pp. 465–470.

[12] W. Yu, J. Rosen, and X. Li, "PID admittance control for an upper limb exoskeleton," in *Proc. Amer. Control Conf.*, 2011, pp. 1124–1129.

[13] W. Yu, R. C. Rodriguez, and X. Li, "Neural PID admittance control of a robot," in *Proc. Amer. Control Conf.*, 2013, pp. 4970–4976.

[14] Z. Liu, F. Wang, and Y. Zhang, "Adaptive visual tracking control for manipulator with actuator fuzzy dead-zone constraint and unmodeled dynamic," *IEEE Trans. Syst., Man, Cybern., Syst.*, vol. 45, no. 10, pp. 1301–1312, Oct. 2015.

[15] Y.-J. Liu, S. M. Lu, and S. C. Tong, "Neural network controller design for an uncertain robot with time-varying output constraint," *IEEE Trans. Syst., Man, Cybern., Syst.*, vol. 47, no. 8, pp. 2060–2068, Aug. 2017.

[16] T. Schmidt *et al.*, "Depth-based tracking with physical constraints for robot manipulation," in *Proc. IEEE Int. Conf. Robot. Autom.*, 2015, pp. 119–126.

[17] S. L. D. Kothare and M. Morari, "Contractive model predictive control for constrained nonlinear systems," *IEEE Trans. Autom. Control*, vol. 45, no. 6, pp. 1053–1071, Jun. 2000.

[18] W. He, Y. Chen, and Z. Yin, "Adaptive neural network control of an uncertain robot with full-state constraints," *IEEE Trans. Cybern.*, vol. 46, no. 3, pp. 620–629, Mar. 2016.

[19] K. P. Tee, S. S. Ge, and E. H. Tay, "Barrier Lyapunov functions for the control of output-constrained nonlinear systems," *Automatica*, vol. 45, no. 4, pp. 918–927, 2009.

[20] B. Ren, S. S. Ge, K. P. Tee, and T. H. Lee, "Adaptive neural control for output feedback nonlinear systems using a barrier Lyapunov function," *IEEE Trans. Neural Netw.*, vol. 21, no. 8, pp. 1339–1345, Aug. 2010.

[21] K. P. Tee, B. Ren, and S. S. Ge, "Control of nonlinear systems with time-varying output constraints," *Automatica*, vol. 47, no. 11, pp. 2511–2516, 2011.

[22] K. P. Tee and S. S. Ge, "Control of state-constrained nonlinear systems using integral barrier Lyapunov functionals," in *Proc. IEEE 51st Annu. Conf. Decis. Control*, 2012, pp. 3239–3244.

[23] W. He and T. Ma, "Adaptive neural network control of a vessel with output constraints using the asymmetric barrier Lyapunov function," *IEEE Trans. Cybern.*, vol. 47, no. 7, pp. 1641–1651, Jul. 2017.

[24] H. Hoffmann, P. Pastor, D.-H. Park, and S. Schaal, "Biologically-inspired dynamical systems for movement generation: Automatic real-time goal adaptation and obstacle avoidance," in *Proc. IEEE Int. Conf. Robot. Autom.*, 2009, pp. 2587–2592.

[25] S. P. Buerger, "Stable, high-force, low-impedance robotic actuators for human-interactive machines," Ph.D. dissertation, Dept. Mech. Eng., Massachusetts Inst. Technol., Cambridge, MA, USA, 2005.

[26] S. Calinon, Z. Li, T. Alizadeh, N. G. Tsagarakis, and D. G. Caldwell, "Statistical dynamical systems for skills acquisition in humanoids," in *Proc. 12th IEEE-RAS Int. Conf. Humanoid Robots*, 2012, pp. 323–329.

[27] L. Rozo, S. Calinon, D. G. Caldwell, P. Jimenez, and C. Torras, "Learning collaborative impedance-based robot behaviors," in *Proc. AAAI Conf. Artif. Intell.*, 2013, pp. 1422–1428.

[28] A. P. Dempster, N. M. Laird, and D. B. Rubin, "Maximum likelihood from incomplete data via the EM algorithm," *J. Roy. Stat. Soc.*, vol. 39, no. 1, pp. 138–145, 1977.

[29] S. Calinon, T. Alizadeh, and D. G. Caldwell, "On improving the extrapolation capability of task-parameterized movement models," in *Proc. IEEE/RSJ Int. Conf. Intell. Robots Syst.*, Tokyo, Japan, Nov. 2013, pp. 610–616.

[30] E. Parzen, *Modern Probability Theory and Its Applications*, 1st ed. Hoboken, NJ, USA: Wiley, 1960.

[31] M. Chen and S. S. Ge, "Direct adaptive neural control for a class of uncertain nonaffine nonlinear systems based on disturbance observer," *IEEE Trans. Cybern.*, vol. 43, no. 4, pp. 1213–1225, Aug. 2013.

[32] W. Meng *et al.*, "NN-based asymptotic tracking control for a class of strict-feedback uncertain nonlinear systems with output constraints," in *Proc. IEEE 51st Annu. Conf. Decis. Control*, 2012, pp. 5410–5415.

[33] J. S. Park, C. Park, and D. Manocha, "Intention-aware motion planning using learning based human motion prediction," in *Proc. Robot. Sci. Syst.*, 2017.

[34] T. Takeda, Y. Hirata, and K. Kosuge, "Dance step estimation method based on HMM for dance partner robot," *IEEE Trans. Ind. Electron.*, vol. 54, no. 2, pp. 699–706, Apr. 2007.

[35] J. von Zitzewitz, M. Bernhardt, and R. Riener, "A novel method for automatic treadmill speed adaptation," *IEEE Trans. Neural Syst. Rehab. Eng.*, vol. 15, no. 3, pp. 401–409, Sep. 2007.

[36] P. R. Culmer *et al.*, "A control strategy for upper limb robotic rehabilitation with a dual robot system," *IEEE/ASME Trans. Mechatron.*, vol. 15, no. 4, pp. 575–585, Aug. 2010.

[37] T. Lenzi, S. M. De Rossi, N. Vitiello, and M. C. Carrozza, "Intention-based EMG control for powered exoskeletons," *IEEE Trans. Biomed. Eng.*, vol. 59, no. 8, pp. 2180–2190, Apr. 2012.

[38] A. Tsukahara, Y. Hasegawa, K. Eguchi, and Y. Sankai, "Restoration of gait for spinal cord injury patients using HAL with intention estimator for preferable swing speed," *IEEE Trans. Neural Syst. Rehab. Eng.*, vol. 23, no. 2, pp. 308–318, Mar. 2015.

[39] D. Cehajic, S. Erhart, and S. Hirche, "Grasp pose estimation in human–robot manipulation tasks using wearable motion sensors," in *Proc. IEEE/RSJ Int. Conf. Intell. Robots Syst.*, 2015, pp. 1031–1036.

[40] H. C. Ravichandar and A. P. Dani, "Human intention inference using expectation-maximization algorithm with online model learning," *IEEE Trans. Autom. Sci. Eng.*, vol. 14, no. 2, pp. 855–868, Apr. 2017.

[41] J.-I. Furukawa, T. Noda, T. Teramae, and J. Morimoto, "Human movement modeling to detect biosignal sensor failures for myoelectric assistive robot control," *IEEE Trans. Robot.*, vol. 33, no. 4, pp. 1–12, Aug. 2017.

[42] W. Wu, Y. Gao, E. Bienenstock, J. P. Donoghue, and M. J. Black, "Bayesian population decoding of motor cortical activity using a Kalman filter," *Neural Comput.*, vol. 18, no. 1, pp. 80–118, 2006.

[43] E. Noohi and M. Žefran, "Estimating human intention during a human–robot cooperative task based on the internal force model," *Trends in Control and Decision-Making for Human–Robot Collaboration Systems*. Cham, Switzerland: Springer, 2017.

[44] M. Maaref, A. Rezazadeh, K. Shamaei, and M. Tavakoli, "A Gaussian mixture framework for co-operative rehabilitation therapy in assistive impedance-based tasks," *IEEE J. Sel. Topics Signal Process.*, vol. 10, no. 5, pp. 904–913, Aug. 2016.

[45] V. K. Narayanan, A. Spalanzani, and M. Babel, "A semi-autonomous framework for human-aware and user intention driven wheelchair mobility assistance," in *Proc. IEEE/RSJ Int. Conf. Intell. Robots Syst.*, 2016, pp. 4700–4707.

[46] A. Pervez and D. Lee, "Learning task-parameterized dynamic movement primitives using mixture of GMMs," *Intell. Service Robot.*, vol. 11, no. 1, pp. 61–78, 2017.

[47] H. Wang and K. Kosuge, "Control of a robot dancer for enhancing haptic human–robot interaction in Waltz," *IEEE Trans. Haptics*, vol. 5, no. 3, pp. 264–273, Jan. 2012.

[48] W. Sheng, A. Thobbi, and Y. Gu, "An integrated framework for human–robot collaborative manipulation," *IEEE Trans. Cybern.*, vol. 45, no. 10, pp. 2030–2041, Oct. 2015.

[49] D. F. P. Granados, B. A. Yamamoto, H. Kamide, J. Kinugawa, and K. Kosuge, "Dance teaching by a robot: Combining cognitive and physical human–robot interaction for supporting the skill learning process," *IEEE Robot. Autom. Lett.*, vol. 2, no. 3, pp. 1452–1459, Jul. 2017.

[50] Y. Huang, K. B. Englehart, B. Hudgins, and A. D. C. Chan, "A Gaussian mixture model based classification scheme for myoelectric control of powered upper limb prostheses," *IEEE Trans. Biomed. Eng.*, vol. 52, no. 11, pp. 1801–1811, Nov. 2005.

Mingdi Deng received the B.S. degree in automation from Northeastern University, Shenyang, China, in 2012. He is currently pursing the master's degree with the College of Automation Science and Engineering, South China University of Technology, Guangzhou, China.

His current research interests include human–robot interaction and motion planning.

Zhijun Li (M'07–SM'09) received the Ph.D. degree in mechatronics from Shanghai Jiao Tong University, Shanghai, China, in 2002.

From 2003 to 2005, he was a Postdoctoral Fellow with the Department of Mechanical Engineering and Intelligent Systems, University of Electro-Communications, Tokyo, Japan. From 2005 to 2006, he was a Research Fellow with the Department of Electrical and Computer Engineering, National University of Singapore, Singapore, and Nanyang Technological University, Singapore. In 2012, he was a Professor with the College of Automation Science and Engineering, South China University of Technology, Guangzhou, China. Since 2017, he has been a Professor with the Department of Automation, University of Science and Technology, Hefei, China. His current research interests include service robotics, tele-operation systems, nonlinear control, and neural network optimization.

Dr. Li has been the Co-Chair of the Technical Committee on Biomechatronics and Bio-robotics Systems, IEEE Systems, Man, and Cybernetics Society, and Technical Committee on Neuro-Robotics Systems, IEEE Robotics and Automation Society, since 2016. He is serving as an editor-at-large for the *Journal of Intelligent & Robotic Systems* and an associate editor of several IEEE TRANSACTIONS. He has been the General Chair and the Program Chair of the 2016 and 2017 IEEE Conference on Advanced Robotics and Mechatronics, respectively.

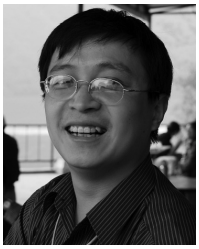

Yu Kang (M'09–SM'14) received the Dr.Eng. degree in control theory and control engineering from the University of Science and Technology of China, Hefei, China, in 2005.

From 2005 to 2007, he was a Post-Doctoral Fellow with the Academy of Mathematics and Systems Science, Chinese Academy of Sciences, Beijing, China. He is currently a Professor with the Department of Automation, and with the State Key Laboratory of Fire Science, and with the Institute of Advanced Technology, University of Science and Technology of China. His current research interests include adaptive/robust control, variable structure control, mobile manipulator, and Markovian jump systems.

C. L. Philip Chen (S'88–M'88–SM'94–F'07) received the M.S. degree in electrical engineering from the University of Michigan, Ann Arbor, MI, USA, in 1985 and the Ph.D. degree in electrical engineering from Purdue University, West Lafayette, IN, USA, in 1988.

He was the Dean of the Faculty of Science and Technology, University of Macau, Macau, China, where he is currently a Chair Professor with the Department of Computer and Information Science. His current research interests include systems, cybernetics, and computational intelligence.

Dr. Chen has been the Editor-in-Chief of the IEEE TRANSACTIONS ON SYSTEMS, MAN, AND CYBERNETICS: SYSTEMS since 2014 and an associate editor of several IEEE TRANSACTIONS. He was the President of IEEE Systems, Man, and Cybernetics Society from 2012 to 2013, the General Chair of SMC 2009 annual conference, and the Program Chair of SMC 2014 in addition to serving as the general/program chair of many international conferences. He is also an ExCom Member of the Chinese Association of Automation (CAA), an Associate Editor-in-Chief for Communication of CAA, the Chair of TC 9.1 Economic and Business Systems of IFAC, and a Program Evaluator of the Accreditation Board of Engineering and Technology in Electrical Engineering, Computer Engineering, and Software Engineering. He is a fellow of CAA, HKIE, and AAAS.

Xiaoli Chu received the B.S. degree in computer science and technology from Jianghuai College, Anhui University, Anhui, China, in 2011 and the M.S. degree in computer system architecture from the Hefei University of Technology, Anhui, in 2014.

She is currently a Research Assistant with the Department of Automation, University of Science and Technology of China, Hefei, China. Her current research interests include mobile robot and neural network control and optimization.